processes

MDPI

Review

Physical and Mathematical Modelling of Mass Transfer in Ladles due to Bottom Gas Stirring: A Review

Alberto N. Conejo

School of Metallurgical and Ecological Engineering, University of Science and Technology, 30 Xueyuan Road, Haidian District, Beijing 100083, China; aconejonava@hotmail.com or aconejo@ustb.edu.cn

Received: 9 April 2020; Accepted: 8 May 2020; Published: 27 June 2020

Abstract: Steelmaking involves high-temperature processing. At high temperatures mass transport is usually the rate limiting step. In steelmaking there are several mass transport phenomena occurring simultaneously such as melting and dissolution of additions, decarburization, refining (De-P and De-S), etc. In ladle metallurgy, refining is one of the most important operations. To improve the rate of mass transfer bottom gas injection is applied. In the past, most relationships between the mass transfer coefficient (*mtc*) and gas injection have been associated with stirring energy as the dominant variable. The current review analyzes a broad range of physical and mathematical modeling investigations to expose that a large number of variables contribute to define the final value of the *mtc*. Since bottom gas injection attempts to improve mixing phenomena in the whole slag/steel system, our current knowledge shows limitations to improve mixing conditions in both phases simultaneously. Nevertheless, some variables can be optimized to reach a better performance in metallurgical ladles. In addition to this, the review also provides a state of the art on liquid–liquid mass transfer and suggests the current challenges in this field.

Keywords: mass transfer coefficient; mixing time; physical modeling; mathematical modeling; kinetic models

1. Introduction

Many studies have been conducted to describe transport phenomena in ladles and the results are summarized in several reviews [1–4]. The previous reviews have included mass transfer to a limited extent. The reviews from Mazumdar et al. [1,2] were focused on solid–liquid systems. Sichen [3] discussed limitations of the two-film theory and Liu et al. [4] summarized mixing phenomena by physical and mathematical modeling due to gas stirring in ladles, indicating that a limited number of studies involved mass transfer. Ghotli et al. [5] reviewed liquid–liquid mass transfer in mechanically stirred vessels. Mechanical and gas stirring involve different operational parameters. In steelmaking, in particular in ladle metallurgy, its rate of production and final steel quality rely on mixing efficiency both liquid steel and liquid slag. The current review will primarily focus on the physical and mathematical modeling work that involves liquid–liquid mass transfer due to bottom gas injection.

The molar flux of species j (N_j) is proportional to the concentration gradient according with Fick's law for diffusion without convection and shown below. This form of the equation is valid for dilute systems, typical of steelmaking. The proportionality constant is the *mass transfer coefficient* (*mtc*). Depending on the experimental conditions the units for the *mtc* can change. To avoid confusion the units are briefly revised. If the concentration units for C_j are in mol/cm^3 then the units for k_j are cm/s [6].

$$N_j = -D_j\left(\frac{\partial C_j}{\partial y}\right) = -\frac{D_j}{\delta_m}\Delta C_j = k_j\left(C_j^b - C_j^{eq}\right) \quad (1)$$

where N_j is the molar flux in mol/cm^2·s, C_j is the concentration in mol/cm^3, D_j is the diffusion coefficient in cm^2/s, y is distance in cm, δ_m is the diffusion boundary layer thickness in cm, k_j is the mass transfer coefficient in cm/s. Superscripts *b* and *eq* represent bulk and equilibrium values, respectively. Subscript j represents a chemical species.

Since the molar flux (N_j) is the amount of material transferred per unit area and unit time, the experimental measurement of the *mtc* requires knowledge of the interfacial area (A). In most cases this value is unknown. In this condition, the mass transfer coefficient is reported as the product, (k_j·A) called *volumetric mass transfer coefficient* (*vmtc*), with units cm^3/min. If the volume of the liquid remains constant, we denote this *vmtc* as $\left(k_j \cdot a\right)$, with units min^{-1}

$$N_j = \frac{1}{A}\frac{\partial n_j}{\partial t} = k_j\left(C_j^b - C_j^{eq}\right) \quad (2)$$

$$\frac{\partial n_j}{\partial t} = V\frac{\partial C_j}{\partial t} = \left(k_j \cdot A\right)\left(C_j^b - C_j^{eq}\right) \quad (3)$$

$$\frac{\partial C_j}{\partial t} = \left(k_j \cdot \frac{A}{V}\right)\left(C_j^b - C_j^{eq}\right) = \left(k_j \cdot a\right)\left(C_j^b - C_j^{eq}\right) \quad (4)$$

The effect of the stirring conditions on the mass transfer coefficient has been experimentally measured for different systems: (i) gas–solid–liquid system: a typical example is the melting of additions by mechanical stirring (solid-liquid system) or by gas stirring (gas-solid-liquid system), (ii) gas–liquid system: some examples are gas absorption from the atmosphere into liquid steel, absorption of elements when different types of gases are injected (nitrogen, carbon dioxide, etc.) or oxygen injection for decarburization, and (iii) gas–liquid–liquid system: the main examples are slag/metal interfacial reactions. To clarify terms used in this work, in the gas–liquid system the gas is a reacting species that dissolves in the liquid in contrast to the gas–liquid–liquid system where the gas is an inert species and where an impurity dissolved in the lower liquid phase diffuses to the upper liquid phase. This review will focus primarily on the study of the *mtc* in the gas–liquid–liquid system, however, as an introduction the other systems are briefly reviewed in the beginning in Sections 2 and 3, followed by a detailed review in Section 4 on liquid–liquid mass transfer involving both physical and mathematical modeling studies. Section 5 provides a final assessment of our current understanding on this subject and suggest guidelines for further research.

2. Mass Transfer during the Melting Rate of Additions (Solid–Liquid and Gas–Solid–Liquid Systems)

The effect of the stirring conditions on the mass transfer coefficient (*mtc*) during the melting rate of additions in ladles has been investigated in detail using a rotating cylinder electrode (RCE) immersed in a liquid and has resulted in many semi-empirical correlations involving dimensionless numbers, as shown in Table 1. Most of these correlations involve three dimensionless numbers; Sherwood (Sh), Reynolds (Re), and Schmidt (Sc). This is the result of a simple dimensional analysis, describing the mass transfer coefficient (k) as a function of the fluid's kinematic viscosity (ν), fluid's velocity (U), diffusivity (D) of transferred species, as well as a characteristic length of the reactor (l), under isothermal conditions.

$$k = f(U, D, \nu, l) \quad (5)$$

This system involves five variables and can be described with two dimensions (L,T), therefore, in accordance with the π-theorem, it can be defined with three π-dimensionless groups, as follows:

$$\pi_1 = k(l)^{a_1}(D)^{b_1} \quad (6)$$

$$\pi_2 = U(l)^{a_2}(D)^{b_2} \quad (7)$$

$$\pi_3 = \nu(l)^{a_3}(D)^{b_3} \quad (8)$$

Applying the principle of dimensional homogeneity, the resulting π-groups are:

$$\frac{kl}{D} = f\left(\frac{Ul}{D}\right)^a\left(\frac{\nu}{D}\right)^b \quad (9)$$

Alternatively:

$$Sh = f\left(Re^a Sc^b\right) \quad (10)$$

If the stirring conditions produce slag emulsification, the previous analysis should be extended to include surface tension [7]. In the mass transfer model developed by Oeters and Xie [8] this relationship holds for two cases under non-turbulent flow; a liquid in contact with a free surface and a liquid in contact with a solid wall. In the first case the velocity at the interface is the same as the velocity in the bulk and in the second case the velocity of the liquid at the interface is zero. Both are limiting cases for the liquid–liquid interface.

The first systematic correlation involving Sherwood (Sh), Reynolds (Re), and Schmidt (Sc) numbers, describing the *mtc* under turbulent flow without gas injection was reported by Eisenberg et al. in 1955. It has been confirmed to remain acceptable for the dissolution rate of iron into liquid steel by subsequent investigations [9–12]. An important parameter is the velocity of the fluid. If the experiments are carried out without gas injection, that velocity can be estimated from the peripheral velocity of the RCE. Under multi-phase flow conditions, the velocity components of the fluid are needed in order to compute the *mtc*. This information can be obtained with the development of mathematical models [13–16], by direct measurements, for example with particle image velocimetry (PIV) or laser doppler velocimetry (LDV) [17], by photographic analysis [18,19], and also with an energy balance [18].

Another group of correlations have been reported using the mass transfer Stanton number (St). It has been applied in the dissolution rate of solid lime into liquid slag [20–22].

The gas injection position is an important variable because it affects mixing phenomena. Wright [23] reported that the dissolution rate of a steel rod under natural convection was higher when placed in the center in comparison with an off-center position, on the contrary Koria [19] reported a higher dissolution rate when the rod was located off-center, under central bottom gas injection conditions. Alloy additions in the ladle should be made under conditions that enhance its melting rate.

Table 1. Mass transfer correlations for solid–liquid and gas–solid–liquid systems.

	Year	Authors	Solid Bar	r/R	Mass Transfer Correlations
1	1955	Eisenberg et al.	$(C_6H_5CO_2H)_{(s)}$	-	$Sh = 0.079Re^{0.7}Sc^{0.356}$
2	1967	Kosaka and Minowa	Steel bar	-	$Sh = 0.064Re^{0.75}Sc^{0.33}$
3	1974	Kim and Pehlke	Iron bar	-	$Sh = 0.112Re^{0.67}Sc^{0.356}$
4	1985	Shigeno et al.	Steel bar	-	$Sh = 0.051Re^{0.78}Sc^{0.33}$
5	1979	Szekely et al.	Graphite bar	0	$Sh = 2 + 0.72Re^{0.75}Ti^{0.25}Sc^{0.33}$
6	1989	Wright	Steel bar *	-	$Sh = 0.13(Gr{\cdot}Sc)^{0.75}$
7	1990	Mazumdar et al.	$(C_6H_5CO_2H)_{(s)}$	0	$Sh = 0.73Re^{0.57}Ti^{0.32}Sc^{0.33}$
8	1992	Mazumdar et al.	Steel rod	0	$k = 7.8 \times 10^{-3}\, Q^{0.19}$
9	2008	Kitamura et al.	Solid lime	-	$St\, Sc^{0.66} = 0.378Re^{-0.31}$

* natural convection, where: $Sh = k_mL/D$, $St = k_m/U$, $Re = \rho UL/\mu$, $Sc = \mu/\rho D$, $Ti = \sqrt{U_{rms}^2}/\overline{U}_0$. k_m is the convective *mtc*, D represents mass diffusivity, μ is the dynamic viscosity of the fluid, ρ is the density of the fluid, U the velocity of the fluid, $\overline{U}_0$ is the velocity at the center line of the rising two phase plume and U_{rms} is the rms or fluctuating velocity.

3. Mass Transfer due to Gas Absorption (Gas–Liquid System)

Gas absorption is an important phenomenon in steelmaking that covers the absorption of undesirable gases from the atmosphere. Maruoka et al. [24] investigated the removal of oxygen by water modeling with different layouts of gas injection. The whole experimental data was described by a relationship between the *vmtc* and the product of the ladle eye times the bubble velocity, subsequently, the *vmtc* was defined in terms of the gas flow rate and the number of nozzles $\left(\propto Q^{0.87}N^{0.13}\right)$. Kato et al. [25] measured the absorption of oxygen in a water model and found that the *mtc* is higher for bottom gas injection in comparison with top gas injection. Another group of studies have been carried out on the absorption of CO_2 in aqueous-NaOH solutions [26,27]. Inada et al. [26] reported that increasing the number of nozzles decreases the *vmtc* per one nozzle. They compared one, three, and five nozzles. These reports found an exponential relationship between the *mtc* and stirring energy, with an exponent in the range from 0.65 to 0.8. Rui et al. [28] also measured the rate of absorption of CO_2 and found that the *mtc* is higher for one oval snorkel in comparison with a circular snorkel, if the nozzle radial position is located between the center and half radius.

Mass transfer in solid–liquid, gas–liquid, and liquid–liquid systems, even if gas stirring is not involved, has many similarities. In all of these systems mass transfer is controlled by diffusion coefficients, velocities (solid, liquid or gas phases), physical properties for the phase involved, etc. At the same time there are important differences. If mass transfer from a solid is involved, the first step is melting and then in a second step is the dissolution process. Mass transfer from a gas phase is different to the case that involves mass transfer due to chemical reaction at the slag/metal interface, not only because the phases involved are different but the chemical reaction itself. The main point is to understand that different variables operate in those processes. In the following sections the review will focus on the previous work that has been developed to identify the variables that affect the rate of mass transfer in gas–liquid–liquid systems.

4. Slag/Metal Interfacial Mass Transfer due to Bottom Gas Injection (Gas–Liquid–Liquid Systems)

4.1. Physical Modeling

The *mtc* in bubble driven systems has been investigated by physical and mathematical modeling and is usually reported as a function of the stirring energy or gas flow rate since these terms are proportional to each other. Table 2 summarizes a large number of correlations between the *mtc* and gas stirring conditions. In addition to ladles, some of the correlations reported include bottom gas injection in other metallurgical reactors like the QBOP.

The first systematic physical modeling work to describe mass transfer as a function of gas injection was conducted by Richardson et al., starting in the late 1960s [29,30]. In one group of experiments [29], bubbles from 3–47 mL were passed through a column containing Hg and aqueous iron chloride. This system can be adjusted to get mass transfer control in either phase. It was found that mass transfer increased with the bubble size and height of the liquid. These authors [30] were the first ones to apply a turbulence theory to describe the *mtc* as a function of gas flow rate and reactor's dimensions. Li and Yin [31] also reported the effect of the bubble size, however instead of the *mtc* increasing with an increase in bubble size they reported a decrease, for nozzle diameters in the range from 1 to 3 mm. Inada and Watanabe [26] as well as Fruehan and Martonik [32] reported that the nozzle diameter has minimal or no effect on the *vmtc*, respectively. Riboud and Olette [33,34] investigated the desulphurization of liquid steel and reported the *mtc* as a function of the specific volumetric gas flow rate across the slag/metal interface, similar to the previous work by Richardson et al.

Up to 1975 mixing phenomena for bubble stirred systems were related with the gas flow rate. In this year Nakanishi et al. reported a correlation between mixing time and stirring energy [35] and eventually this idea was also used to report correlations between mass transfer and stirring energy. Stirring energy is directly proportional to the gas flow rate $(\varepsilon \propto Q^n)$. The exponent n is close to the

unity [36]. This result can be theoretically derived from a relationship reported by Asai et al. [37] where $\varepsilon \propto U^3$ and the experimental data from Lehner et al. [38] where $U \propto Q^{1/3}$, then $\varepsilon \propto Q$. Engh and Oeters have also confirmed the linear relationship [39,40]. Many equations have been reported to compute stirring energy as a function of gas flow rate [41], one that is simple and accurate was reported by Mazumdar and Guthrie [42], as follows:

$$\varepsilon = \frac{\rho_l g H_l Q}{\rho_l \pi R^2 H_l} = \frac{gQ}{\pi R^2} \quad (11)$$

where ε is stirring energy in Watts/ton, ρ_l is the density of the liquid in ton/m^3, g is the acceleration due to gravity at the surface of Earth, 9.81 m/s^2, H_l is the height of the liquid in m, R is the radius of the reactor in m, Q is the gas flow rate in Nm^3/s.

Nakanishi et al. [43] reported results from a water model scaled from a Q-BOP indicating a change in the rate of mass transfer at about 80 Nl/min with bottom gas injection. Ishida et al. [44] and Berg et al. [45] also reported a change in the rate of mass transfer for a slag/metal system and in both cases a sharp transition for a stirring energy at 60 Watt/ton was reported. Umezawa et al. [46,47] employing also a steel/slag system and a much larger range in stirring energies did not report a change in the rate of mass transfer. Similar results were reported in a subsequent study with mechanical stirring [47]. In addition to correlations between the *mtc* and stirring energy, Clinton et al. [48] found a relationship between the *mtc* and the superficial velocity, and Minda et al. [49] found that increasing the volume of slag increases the *mtc*, conducting experiments at high stirring conditions.

In 1983 Asai et al. [37] published a review with 12 correlations including their own water modeling work. They analyzed the value of the exponent on the stirring energy by increasing the gas flow rate and suggested a drastic change from about 0.25 to more than unity, at about 450 W/m^3 (60 W/ton). They also analyzed that the low value can be predicted by the penetration theory under laminar flow. This work was updated to 15 correlations in 1988 [50]. This work clearly shows that gas flow rate is one of the main variables affecting the rate of mass transfer. Patel et al. [51] used an aqueous-NaOH solution covered by hexane and iodine dissolved in water as a tracer, which, when transferred into hexane it changes color to violet. The iodine equilibrium concentration was reported as 0.081% for an initial concentration of 0.16%. Their results were explained on the basis of Higbie's penetration theory.

The rate of mass transfer can change as a function of the gas flow rate. The change in slope is defined with a different correlation. Sawada et al. [52] reported one single correlation to describe the *mtc* including the reactor diameter to summarize their water modeling results. Ooga et al. [53] reported one change of slope that increased as the gas flow rate also increased. In this work slag emulsification was evident at a critical gas flow rate. The critical gas flow rate increased from 0.6 to 1.2 Nl/min by increasing the diameter of the ladle from 11 to 18 cm. Endo et al. [54] reported three changes in the slope, from low to high and then low again. Hirasawa et al. [55–59] carried out experiments at high temperatures analyzing the effect of reactor diameter, gas flow rate, height of liquid, and slag thickness. They reported three slopes. The slope decreased from the first to the second region at a critical gas flow rate and then increased again from the second to the third region. A strong slag emulsification was observed only in the third region. For the first region the critical gas flow rate changed with reactor diameter. The increase of the *mtc* in the third region was attributed to slag emulsification. They explained that in region two the motion of the slag increased but led to suppression of the motion of the lower phase due to a higher slag viscosity and a large interfacial tension. They reported that increasing the height of the liquid up to a H/D ratio of one, the *mtc* also increased and then remained constant, in regions one and two. Their work was the first attempt to unify all experimental data applying Davies theory of turbulence. Mukawa et al. [60] also reported a similar correlation for the *mtc*.

Fruehan et al. [61–63] investigated for the first time the relationship between mass transfer and mixing time in a ladle. They analyzed the following variables: gas flow rate, number of nozzles, nozzle radial position, slag volume, slag viscosity, and nozzle diameter. Mixing time is a parameter that measures the mixing efficiency of the primary phase (liquid steel), on the other hand, mass transfer

measures the diffusion of species from the primary phase to the upper slag layer. Although both phenomena are affected by the mixing conditions, the final effect of the gas injection system can have dramatically different effects. Their conclusions are listed below:

i At high gas flow rates mixing time and mass transfer cannot be improved simultaneously. Mass transfer is improved with central gas injection because the slag layer has better mixing conditions, however this position is the worst case for mixing liquid steel. At low gas flow rates, the rate of mass transfer is independent of the gas injection layout.

ii Mass transfer shows three slopes that increase as the gas flow rate (Q) also increases. The change in slope is due to slag emulsification and occurs at about 5.3 W/ton. The nozzle diameter and slag viscosity do not have any effect at low Q but at high Q a decrease in slag viscosity and an increase in the nozzle diameter increase the *mtc*. When the slag viscosity increases it also increases the critical gas flow rate for slag emulsification. The authors also reported that increasing the slag thickness, at any Q, the *mtc* increases.

Figure 1 shows the results reported by Kim and Fruehan [61] on mixing time and mass transfer for central and off-central gas injection. It is clear that central gas injection has poor mixing conditions in the bath but on the other hand, the mass transfer coefficient is higher for central gas injection, an indication of better mixing conditions in the slag layer.

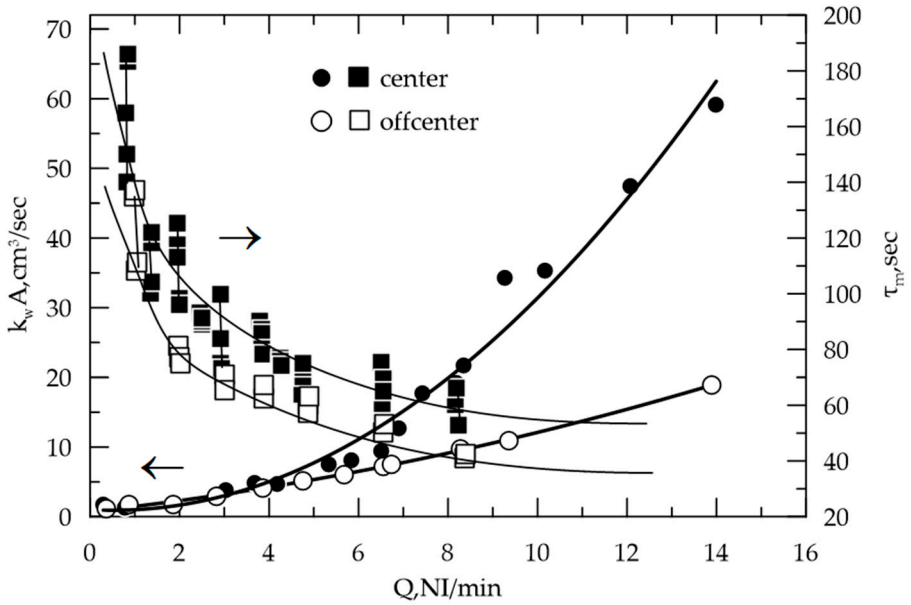

Figure 1. Effect of gas flow rate on both mixing time and the mass transfer coefficient, comparing central and off-central gas injection. Adapted from Kim and Fruehan [61].

Tata steel researchers reported that mixing time and mass transfer can be improved simultaneously applying a gas injection layout that involves differential gas flow rates in each nozzle, however this finding was not reported for a ladle but for a QBOP converter [64]. The stirring conditions in both reactors are quite different as will be explained below. They applied three configurations and the best case was defined when the gas flow rate was linearly increased from one side to the opposite side, using eight nozzles located at about 58% of the radius of the bottom.

Mietz et al. [65] reported results from three different geometric scale ladles using centric and eccentric gas injection. They confirmed that centric gas injection yields a higher rate of mass transfer in particular if a critical gas flow rate for emulsification is exceeded. The critical stirring energy in the three water models was about 15 W/ton. A further analysis also indicated that emulsification is much higher with centric gas injection in comparison with eccentric gas injection [66].

There are few studies regarding the effect of the number of nozzles in ladles on the *mtc*. Endo et al. [54] reported that the rate of mass transfer is higher with two porous plugs in comparison with one porous plug, in particular at high gas flow rates. The same report also cites a work from Aichi steel confirming similar results. A more recent work by Lou and Zhu [67] compared the desulphurization (DeS) ratio in a ladle with one and two nozzles and found that two nozzles (180° separation angle) yield a higher DeS ratio (48%), compared to 46% for central gas injection and 44% for off-center gas injection.

Koria et al. [68–70] studied mass transfer in a water model from a QBOP process. Under similar experimental conditions they reported two different correlations with exponents on the stirring energy of 0.4 and 1. These authors noticed the different time scales between mixing time and mass transfer. The time scale for mass transfer is higher than that for mixing time. Oeters et al. [71] conducted mass transfer experiments on desulphurization at high temperatures. They applied the boundary layer theory to predict the *mtc* with a very good agreement and also reported a change in slope due to slag emulsification at a critical stirring energy of about 4 W/ton. Kitamura et al. [72] reported data for high temperature experiments describing a correlation for the *mtc* in terms of the dimensions of the reactor and also reported a value of activation energy for the rate of desiliconization of hot metal. Koria [73] reported water modeling results on *mtc* for top and bottom gas injection in a QBOP model, defining a correlation that indicates the contribution from both top and bottom gas injection. The work reported by Lachmund et al. [74,75] on an industrial ladle furnace indicates a linear relationship between the *mtc* and stirring energy, one special feature in this work is the large values on stirring energies up to 200 W/ton at atmospheric pressure that led to a large slag emulsification. Most probably the authors have used the gas flow rate at (TP) and not (STP) conditions, which would explain such a high value. They reported the formation of approximately 5×10^7 slag droplets, which increased the surface area up to 173 m^2. Sulasalmi et al. [76] and Senguttuvan and Irons [77] reported the relationship between a liquid's velocity and the generation rate of the interfacial area and residence time of the slag droplets due to slag emulsification.

Gas injection in an industrial ladle furnace is carried out by porous plugs, however, most of the physical modeling work is carried out using nozzles. Few investigations have compared mixing phenomena with both injection elements. Stapurewicz and Themelis [78] compared mass transfer from a gas phase into a liquid with both injection systems and found a higher absorption rate with a porous plug due to the formation of fine bubbles in a water model that largely increase the reaction interface (up to 230%), this result however could be misleading because bubble formation from a porous plug in a water model is different to the argon/liquid steel system. The bubbles in a gas/metal system are bigger because of the non-wetting conditions and their final volume is dominated by the properties of the fluid. An example of the large differences in physical properties in both systems is the surface tension/density ratio; for the air/steel system is three times higher in comparison with the air/water system, 251 and 73, respectively [79]. Mori [80] has even questioned the results from water models to describe high-temperature slag/metal systems on the basis of a low interfacial tension for the water/oil system in comparison with slag/metal systems.

The effect of pressure on the *mtc* has not been considered in the previous correlations since the ladle furnace works under atmospheric conditions, however, the same ladle can operate under vacuum when transferred to the RH or tank degasser stations. The effects of gas stirring under vacuum are enhanced because there is a considerable increment in the bubble size and therefore for the same gas flow rate the *mtc* increases in comparison with atmospheric conditions. Lachmund et al. reported that gas stirring is five times more intense under vacuum (less than 4 mbar) compared with atmospheric conditions [74]. Under vacuum conditions, Sakaguchi and Ito [27] found a correlation of the form $ka \propto \varepsilon^{0.71}$.

From Table 2, it can be seen that using physical modeling to study mass transfer the results are generally expressed by two relationships, on the contrary, for a steel-slag system there is in general only one relationship. The reason for this behavior is the formation of an oil emulsion at a critical

gas flow rate in the oil–water system. Understanding this phenomenon is extremely important to explain mass transfer. As emulsification increases the surface area between oil and water also increases and therefore the rate of mass transfer rate increases. Oil emulsification occurs when the difference in density between oil and water phases is small [50,81]. In a water model the density ratio (water/oil) is close to one and in a few cases can reach up to 1.5, on the contrary, for the steel/slag system the density ratio (steel/slag) is higher than 2.5. Therefore, while in a water model it is easy to form an emulsion in a real steel/slag system it is more difficult.

Asai et al. [50] developed a model to predict slag emulsification based on an energy balance. The critical metal velocity for slag emulsification was defined for the condition when the kinetic energy exceeds the sum of surface energy and energy due to buoyancy. The critical velocity was found to decrease from about 35 to less than 20 cm/s when the density ratio decreases. Since the density ratio in a water model is lower than in the real steel/slag system, it emulsifies with lower velocities. Later on, Wei and Oeters [82] in 1992 reported a robust theoretical model that predicts the rate of slag droplets formation and its size from the interfacial velocity. Savolainen et al. [83] studied in detail the effects of slag thickness (h_s), density differences ($\Delta\rho$), oil viscosity (μ), and interfacial tension (σ) of three oil/water systems on slag emulsification. They reported that both the critical velocity for emulsification and droplet size increases by increasing h_s, μ, and σ, on the other hand, increasing $\Delta\rho$ also increases the critical velocity but the droplet size decreases. It should be noted that these results were obtained employing oils with densities close to water. In addition to the physical properties of the liquids, the critical gas flow rate or liquid velocity also change depending on nozzle position [66].

In some metal/slag systems slag emulsification has been reported [44,45], however in most of these cases this is because they reproduce conditions of the BOP where the rates of gas injection are very high and lead to the formation of slag emulsions but this is not the case of ladle furnace conditions. In a ladle furnace, for example a ladle of 210 ton of nominal capacity with top diameter of 384 cm, bottom diameter 351 cm, and height of liquid steel of 283 cm, operating with two porous plugs and a maximum gas flow rate in each plug of 40 Nm^3/hr (approximately 12 N*l*/min·ton), the maximum stirring energy is about 20 W/ton. This is an extremely high value that produces a large ladle eye and should not be used for a long time. This upper value on stirring energy can be taken as a reference to understand slag emulsification in the previous studies. Several of those studies indicated a critical stirring energy of 60 W/ton to promote slag emulsification, if this is the case then it should be more appropriate of a BOP but not for ladle furnace conditions. For ladle furnace conditions, the reported values from 4 to 6 W/ton would be more appropriate to define the onset for slag emulsification. As a general rule, in the relationships of the form $k \propto Q^n$, the value of n would be less than one if slag emulsification is not present.

Several tracers have been used to measure the *mtc*. In a ladle furnace the main impurity to be removed during steelmaking is sulphur. It is also known that the rate of desulphurization from liquid steel follows first order kinetics, therefore in a water model the tracer should behave similar to sulphur not only in terms of its partition ratio but also show a similar order of reaction to simplify the analysis of the *mtc*. The sulphur partition ratio (L_S) is in the range from 100 to 500 under equilibrium conditions [84–86]. In practice this value ranges from 20 to 100 depending on the stirring conditions and slag chemical composition [87]. Koria et al. [73] has reported that the partition ratio of benzoic acid between water and paraffin oil was 4.5. Kim and Fruehan [61] reported that thymol dissolved in water in contact with a mixture of paraffin oil–cotton seed oil (50/50) can reach a partition ratio higher than 350 and therefore it was suggested as an ideal tracer. The author has undertaken extensive work with a similar system and the maximum value was in the order of 50. Mietz et al. [66] used a mixture of iodium and potassium iodide dissolved in water and in contact with cyclohexane, reaching a partition ratio of 10. The magnitude of the *mtc* will depend on the type of tracer, its initial concentration, and the final equilibrium concentration.

Table 2. Correlations between *mtc* (or *vmtc*) and stirring energy ε (W/ton) or Q (Nl/min).

	Year	Authors	Process	System	Tracer	Gas	Correlation	ε
1	1968	Subramanian and Richardson	L-L column	In (Hg)–Fe^{2+}(H_2O)	Indium	Air	$k \propto V_b^{0.42}$	$3 < V_b < 47$ mL
2	1969	Patel et al.	L-L column	Water–hexane	Iodine	N_2	$k \propto Q^{0.72}$	$0.08 < Q < 0.4$
3	1974	Richardson et al.	L-L column	Molten salt–lead	Pb^{2+}	-	$k \propto \left(Q/d_c^2\right)^{0.5}$	-
4	1980	Lehner et al.	60 ton ladle	Steel–slag	Cu	Ar	$k \propto Q^{0.33}$	$8.3 < Q < 83.3$
5	1980	Nakanishi et al.	(Q-BOP)	Water–paraffin	Naphtol	Air	$kA = 3.7Q^{0.36}$	$30 < Q < 80$
							$kA = 1.5\times10^{-5}Q^{3.0}$	$80 < Q < 200$
6	1981	Ishida et al.	2.5 ton (LMF)	Steel–slag	Sulphur	Ar	$ka = 0.013\varepsilon^{0.25}$	$\varepsilon < 60$
							$ka = 8\times10^{-6}\varepsilon^{2.1}$	$\varepsilon > 60$
7	1981	Umezawa et al.	Mech and gas	Steel–slag	P	Ar	$ka = 1.56\varepsilon^{0.60}$	$40 < \varepsilon < 280$
8	1982	Clinton et al.	Contactors	Water–mercury	Quinone	N_2	$k \propto U_s^{0.6-0.8}$	$0.06 < Q < 0.4$
9	1982	Riboud- Olette	Ladle	Steel–slag	S	Ar	$k = 500\left(\frac{D_s Q}{A}\right)^{3.0}$	-
10	1983	Minda et al.	Ladle	Steel–slag	Cr_2O_3	Ar	$kA \propto \varepsilon^{0.9}$	$\varepsilon > 5000$
11	1983	Umezawa et al.	Mech. stirring	Steel–slag	P	-	$ka = 0.14\varepsilon^{0.58}$	$300 < \varepsilon < 2800$
12	1983	Asai et al.		Water–tetraline	Benzoic acid	Air	$ka \propto \varepsilon^{0.36}$	$Q < 150$
							$ka \propto \varepsilon^{1.0}$	$150 < Q < 650$
13	1984	Sawada et al.	Ladle	Water–paraffin	Naphtol	Air	$k \propto (\varepsilon/d_c)^{0.5}$	$1 < \varepsilon < 20$
14	1985	Berg et al.	6 ton ladle	Steel–slag	Sulphur	Ar	$k \propto \varepsilon^{0.3}$	$\varepsilon < 60$
							$k \propto \varepsilon^{1.3}$	$\varepsilon > 60$
15	1985	Schlarb-Frohberg	BOP	Water–white oil	Caprylic acid	Air	$kA = 3.7\times10^{-5}Ar^{0.9}$	$Q < 700$
16	1985	Ooga et al.	ladle	Water– benzene	Benzoic acid	N_2	$kA = \varepsilon^{0.66}$	$Q < 0.6$
							$kA = \varepsilon^{1.1}$	$0.6 < Q < 3$

Table 2. *Cont.*

	Year	Authors	Process	System	Tracer	Gas	Correlation	ε
17	1985	Endo et al.	VOD	Water– benzene	Cu^{2+}		$kA \propto \varepsilon^{0.4}$	$\varepsilon < 4$
							$kA \propto \varepsilon^{0.9}$	$4 < \varepsilon < 20$
18	1987	Hirasawa et al.	ladle	Cu (Si)–slag	Si	Ar	$k \propto \left(\varepsilon / d_c^2\right)^{0.5}$	$Q < 1$
19	1987	Kim and Fruehan	Ladle	Water(paraffin/cotton seed oils)	Thymol	Air	$kA = \varepsilon^{0.6}$	$Q < 5$
							$kA = \varepsilon^{2.51}$	$5 < Q < 12$
20	1988	Koria and George	BOP	Water–paraffin	Benzoic acid	Air	$ka \propto Q^{0.449}$	$1.4 < Q < 5$
21	1989	Matway et al.	BOP	Water–paraffin	Naphtol	Air	$kA \propto Q^{0.91}$	$10 < Q < 100$
22	1989	Wright	Ladle	Steel–slag	Carbon	N_2	$k \propto Q^{0.21}$	$Q < 6$
23	1990	Koria and Pal	BOP	Water–paraffin	Benzoic acid	Air	$ka = 2.8\times10^{-3}\varepsilon^{1.05}$	$1.1 < Q < 6.2$
24	1990	Dang and Oeters	Ind. furnace	Steel–slag	Sulphur	Ar	$k = 8.3\times10^{-5}Q^{0.168}$	$0.2 < \varepsilon < 35$
25	1991	Kitamura et al.	Ind. furnace	Steel–slag	P	Ar	$k \propto \left(\varepsilon\ H^2/D\right)^{0.5}$	$\varepsilon > 60$
26	1992	Koria	QBOP	Water–paraffin	Benzoic acid	Air	$k \propto (\varepsilon_b)^{0.76}(\varepsilon_t)^{0.78}$	$1 < Q < 15$
27	1995	Mukawa et al.	BOP	Steel–slag	P, Si	Ar	$k \propto \left(\varepsilon / d_c^2\right)^{0.7}$	$6 < Q < 1\times10^5$
28	1995	Xie and Oeters	ladle	Steel–slag	P, Si	Ar	$k_i \propto Q^{0.168}$	$0.4 < \varepsilon < 27$
29	1996	Li and Yin	Glass	Hg–$ZnFe^{2+}(H_2O)$	Fe^{2+}	Air	$k \propto \left(Q / d_n^{0.33}\right)^{0.05}$	$0.05< Q < 0.02$
30	2003	Lachmund et al.	ladle	Steel–slag	S	Ar	$k \propto \varepsilon$	$5 < \varepsilon < 300$

where k is the mass transfer coefficient in units length/time, k*a* and kA are volumetric mass transfer coefficients with units; $time^{-1}$ and $lenght^3$/time, respectively, ε is stirring energy in W/ton, ε_b represents stirring energy from bottom gas injection, ε_t represents stirring energy from top gas injection, Q is the gas flow rate in Nl/min, U_s is the superficial velocity, d_c is the diameter of the crucible or reactor, d_n is the nozzle diameter in mm. Due to the broad number of studies, units should be checked in the original sources.

All equations in Table 2, except one, do not include the nozzle diameter which could be an indication that the inlet kinetic energy is not relevant. Lehrer reported that 96% of the inlet kinetic energy is consumed at the orifice region and only 6% is transferred to the liquid [88]. Taniguchi et al. [18] and Wright [23] also found similar results. On the other hand, the effect of the nozzle diameter on mass transfer has been reported by Kim and Fruehan [61] and Jiang et al. [89], for a liquid–liquid–gas and gas–liquid system, respectively. In the first case, the rate of mass transfer increased with an increase in nozzle diameter from 2 to 4.8 mm but only at high gas flow rates, and in the second case decreased when the nozzle diameter was increased from 1 to 3 mm and then remained almost constant with nozzle diameters up to 7 mm.

To define the activation energy for mass transfer requires information on the *mtc* as a function of temperature. Robison and Pehlke studied the reduction of chromium oxide from the slag [90]. They indicated that if the reaction rate is controlled by the interfacial chemical reaction and the area remains constant then a change in the stirring energy will not change the reaction rate, and also defined a range from 65 to 100 kcal/mole if the controlling mechanism is mass transfer from the slag phase and 20 kcal/mole if it is due to mass transport in the metal phase. Kitamura et al. [72] reported an activation energy of 30 kcal/mol for the rate of desiliconization of hot metal and Kang et al. [91] a value of 28 kcal/mol for the oxidation of aluminum by silica from the slag.

The *mtc* is an essential component in the development of a kinetic model, for example, when dealing with the desulphurization rate in the ladle furnace. The previous expressions from Table 2 can be used to simplify the calculation of the metal mtc (k_m). In general mass transfer is controlled by diffusion from the primary steel phase, therefore only k_m is needed. If the process is controlled by diffusion in both phases, the slag mass transfer coefficient is also required. A practical approach that has been used in many investigations [72,92–94] is to assume that the slag *mtc* (k_s) is 10 times slower compared with the steel

$$k_s = k_m/10. \quad (12)$$

Mukawa et al. [60] confirmed this relationship by empirically adjusting parameters in a mathematical model.

Table 3 summarizes the main findings obtained by the previous physical modeling work. It is important to notice the large number of variables that affect the rate of mass transfer.

Table 3. Effect of process variables on the mass transfer coefficient (*k*) due to bottom gas injection in ladles.

Gas flow rate or stirring energy	Q or ε	*k* increases with gas flow rate (or stirring energy). Change in *k* at critical Q for slag emulsification.
Nozzle's radial position	r/R	*k* increases with central gas injection and decreases if the nozzle is off center
Bubble diameter	d_B	*k* increases with large bubbles (9–20 mm) and decreases with small bubbles (1–3 mm)
Nozzle diameter	d_n	Mixed results; it has no effect, *k* increases by increasing d_n at high Q, *k* decreases by increasing d_n
Superficial velocity	U_s	*k* increases with the superficial velocity of the liquid
Slag volume	W_s	*k* increases with the volume of slag
Reactor's diameter	d_c	*k* increases with the reactor diameter
Slag viscosity	μ_s	*k* increases by decreasing the slag viscosity, at high Q
Liquid's height	h_m	*k* increases by increasing the height of the liquid metal up to a critical value
Type of nozzle	-	*k* in one report was higher for porous plugs in comparison with nozzles for the case of gas–liquid mass transfer
Number of nozzles	N	*k* increases with number of porous plugs, from one to two

4.2. Mathematical Modelling of Mass Transfer in the Ladle

The *mtc* can be determined empirically through experimental work by physical modeling. This approach has several limitations: (i) lacks generality; is valid for specific cases, (ii) in general is a constant value, (iii) it is usually reported only in terms of one variable; stirring energy.

In order to overcome the previous limitations, the *mtc* has been explained and derived theoretically with different models. Application of this models to the entire gas/steel/slag system requires the development of numerical solutions. There are three main mass transfer theories:

(1) The film theory developed by Lewis and Whitman [95]. It is the simplest and most commonly used theory. Most of the experimental determination of the *mtc* is based on this theory [61,71]. It assumes that mass transfer occurs on both sides of the interface, flow is in steady state, and the equilibrium conditions are instantaneously reached at the interface. On these assumptions the following relationships are derived:

$$N_{i,m} = -D_{i,m}\frac{\partial C_{i,m}}{\partial y} = -D_m\frac{\left(C^m_{i,int} - C^m_{i,b}\right)}{\delta_m} = N_{i,s} = -D_s\frac{\left(C^s_{i,b} - C^s_{i,int}\right)}{\delta_s} \quad (13)$$

$$\text{if, } L = \frac{C^s_{i,int}}{C^m_{i,int}}$$

$$k = \frac{D}{\delta}, k_m = \frac{D_m}{\delta_m}, k_s = \frac{D_s}{\delta_s}, \text{ then}$$

$$N_i = \frac{k_m k_s}{k_s + k_m/L}\left(C^m_{i,b} - \frac{C^s_{i,b}}{L}\right) = k_o\left(C^m_{i,b} - \frac{C^s_{i,b}}{L}\right) \quad (14)$$

$$k_o = \frac{1}{\frac{1}{k_m} + \frac{1}{k_s L}} \quad (15)$$

where $C^j_{i,int}$ is the concentration at the interface on the side of the j-phase, L is the partition equilibrium ratio, δ is the thickness of the diffusion boundary layer, k_m is the *mtc* for species i in the metal phase, k_s is the *mtc* for species i in the slag phase and k_o the overall *mtc*. If the partition ratio (L) is large the second term can be neglected and the process is controlled by mass transfer in the metal phase. Kang et al. [96] reported that the partition ratio for sulphur should be higher than 100 to assume mass transfer control. Although metal mass transfer control is the most common case in steelmaking, slag mass transfer control or mixed control is also possible. Deo and Boom [97] suggested slag mass transfer control under the following conditions: (a) when the bulk slag phase is pre-saturated with the element to be transferred from the metal and the concentration of the element in the metal phase is high, (b) when the slag is highly viscous and has poor mixing conditions so that $k_s << k_m$, (c) when the reaction product layer that forms on the slag side is solid, so that it does not allow for proper homogenization of the bulk slag phase, (d) when the slag has a low sulfide capacity. Notice that based on the boundary layer theory, the *mtc* is proportional to D to the first power; $k_i \propto D$.

(2) The penetration theory was developed by Higbie [98] and assumes that liquid packets at the interface are periodically renewed by new fresh fluids coming from the bulk, each fluid packet is in contact with the interface for a given time. The boundary layer thickness is much larger than in the film theory. For the metal phase:

$$N_{i,m} = -D_{i,m}\frac{\partial C_{i,m}}{\partial y} = \sqrt{\frac{4D_{i,m}U}{\pi L}}\left(C^m_{i,int} - C^m_{i,b}\right) = k_m\left(C^m_{i,int} - C^m_{i,b}\right) \quad (16)$$

$$k_m = \sqrt{\frac{4D_{i,m}}{\pi\, t}} \tag{17}$$

where t is the contact time of surface renewal. Its value is specific for a given system. Notice that based on the penetration theory, the *mtc* is proportional to the square root of D; $k_i \propto D^{1/2}$. Szekely [99] derived an alternate form of the *mtc* that gives a similar result to the penetration theory. He first derived an expression for heat transfer at the slag/metal interface due to bubble stirring under transient conditions and then applied the same treatment to mass transfer. The final result is expressed in terms of the diffusion coefficients, the equilibrium partition ratio, and the time interval between the arrival of two successive bubbles (t_e).

$$k_m = \left\{1+\frac{1}{L}\left(\frac{D_{i,m}}{D_{i,s}}\right)^{\frac{1}{2}}\right\}^{-1}\sqrt{\frac{4D_{i,m}}{\pi\, t_e}} \tag{18}$$

The time interval, t_e, was computed from the number of bubbles produced per unit time (N_b), the cross-sectional area of the bath (A_B), and the projected area of the bubble (A_b)

$$t_e = \frac{A_B}{A_b N_b} \tag{19}$$

The specific value of the time interval depends on the phenomenon investigated, for example Bafghi et al. [100] defined its value as a function of the frequency of CO formation due to the reduction of FeO during slag foaming and the final expression for the *mtc* was defined in terms of the mass of slag and FeO.

(3) Surface renewal theories: there is a large number of models that propose how to estimate the contact time of surface renewal. Danckwerts [101] suggested that this time is not constant and follows a normal distribution, t is replaced by a parameter s that defines the rate of replacement. Dong et al. [102] found this parameter to be the ratio between the normal fluctuating velocity U_o, at a depth l_o

$$k_m = 0.4\sqrt{\frac{D_{i,m}U_o}{l_o}}. \tag{20}$$

The Large Eddy Model (LEM) suggested by Fortescue and Pearson [103] assumes that the larger eddies are dominant on mass transfer because they contain most of the turbulent energy,

$$k_m = 0.4\sqrt{\frac{D_{i,m}U_{rms}}{l}}. \tag{21}$$

where U_{rms} is the rms velocity of the turbulence and l is the length scale of the large eddies.

Kolgomorov [104] in 1941 formulated the modern concepts of turbulence analyzing the interaction between large and small eddies "decaying" into one another, stating that the small eddies are statistically homogeneous and isotropic. Based on his derivation of length scale and velocity scale, the exposure time can be defined. Applying this concept Banerjee et al. [105] as well as Lamont and Scott [106] suggested that the eddies in the boundary layer are usually small in size and therefore more important. The Small Eddy Model (SEM) is defined by the following equation

$$k_m = 0.4\sqrt{D_{i,m}}\left(\frac{\varepsilon}{\nu}\right)^{0.25}. \tag{22}$$

where $D_{i,m}$ is the molecular diffusivity, ε is the energy dissipation rate, and ν is the kinematic viscosity. A similar equation was also reported by Miyauchi and Kataoka [107] and Ruckenstein [108], with different constants.

According with the surface renewal theories, k is proportional to the square root of the diffusion coefficient. Since the $D_{i,s}$ of the slag is approximately two orders of magnitude of that of the metal, $D_{i,m}$, we get $k_s = k_m/10$. This is another way to validate Equation (12).

Banerjee et al. [109] have proposed equations for both large and small eddies. The small eddies model for un-sheared interfaces when the far-field turbulence is homogeneous and isotropic, was called the Surface Divergent Model (SDM), defined as follows

$$k_m = 0.3U_L\sqrt{D_{i,m}}(ScRe_t)^{-0.5}\left[0.3\left(2.83(Re_t)^{\frac{3}{4}}-2.14(Re_t)^{\frac{2}{3}}\right)\right]^{\frac{1}{4}}. \quad (23)$$

The previous mass transfer models have been compared. Theofanous et al. [110] found that LEM and SEM give good results at small and large turbulent Reynolds numbers, respectively. De Oliveira reported similar results for LEM and SDM [111].

The mathematical models developed to study mixing and mass transfer in ladles is extensive [4,112]. In a mathematical model the velocities of the fluids can be computed allowing the use of the previous mass transfer theories. The simplest numerical modeling approach to study mass transfer under isothermal conditions involves two main parts; development of a fluid dynamics model coupled with a mass transfer model. There are three well defined numerical algorithms; Quasi-single or pseudo-single-phase, Eulerian-Lagrangian (E-L) and Eulerian-Eulerian (E-E). Depending on the commercial code, they can assume different names, for example in ANSYS-Fluent the Lagrangian algorithm is called discrete particle model (DPM). The volume of fluid (VOF) model is a separate Eulerian algorithm that allows to track interfaces. In the most recent mathematical models [67,76,77,113], liquid steel and liquid slag are usually described by an Eulerian algorithm, its interface by the VOF algorithm, and the motion of the bubbles by a Lagrangian algorithm. The governing equations can be described by the following general transport equation for multiphase flow

$$\frac{\partial(\alpha_i\rho_i\phi_i)}{\partial t}+\nabla\cdot(\alpha_i u_i\phi_i) = \nabla\cdot\left(\alpha_i\Gamma_{\varnothing_{i,i}}\nabla\phi_i\right)+\alpha_i S_{\varnothing_i}. \quad (24)$$

where ϕ_i is the variable to be solved, α_i is the volume fraction of the phase, ρ_i is the density of the phase, u_i is the velocity, $\Gamma_{\varnothing_{i,i}}$ is the exchange coefficient, t is time, and S is the source term associated with the creation or destruction of ϕ_i. In the species transport equation, the source term is the rate of mass transport.

Once the flow reaches steady state the mass transfer model is solved. It can be solved only to compute the *mtc* or coupled with a kinetic model to predict, for example, the rate of desulphurization. The numerical calculation of *mtc's* can be made using empirical correlations or with the use of mass transfer theories.

The first numerical models involving mass transfer used a Quasi single-phase approach and axisymmetric gas injection, for example Mazumdar et al. [15] computed the fluid's velocity and then used a previously developed empirical correlation to compute the *mtc*. Costa and Tavares [114] used a similar approach. Ahmadi et al. [115–117] did measurements on the melting rate of a Si rod in liquid aluminum and also developed a 3D numerical model. They applied Mazumdar's correlation to predict the *mtc*. The results gave a similar order of magnitude but the correlation underpredicted the experimental data. They also modified the correlation proposed by Churchill and Bernstein [118] for forced convection, adding the turbulent Reynolds number, reporting some improvements with the following correlation

$$\overline{Sh} = 0.3+\frac{0.62Re_d^{\frac{1}{2}}Sc^{\frac{1}{3}}}{\left[1+(0.4/Sc)^{\frac{2}{3}}\right]^{\frac{1}{4}}}\left[1+\left(\frac{Re_d}{282,000}\right)^{\frac{5}{8}}\right]^{\frac{4}{5}}Re_T^{0.066}. \quad (25)$$

Taniguchi et al. [119] calculated the *mtc* applying both the small-eddy model and the penetration theory for a gas–liquid system. The velocity predictions were validated with experimental data using LDV. The time of surface renewal was estimated from the ratio $(\text{diameter/velocity})_{\text{bubble}}$. They found better agreement with the experimental data in the plume region using the small-eddy model. Lou and Zhu [120], Cao et al. [121], Hoang et al. [122], and Karouni et al. [123] have also reported a good agreement using the small eddy model. Cao et al. [121] employed a diffusivity value for the species in the metal side of 7.0×10^{-9} m^2/s and two orders of magnitude lower for the species in the slag side, 7.0×10^{-11} m^2/s.

De Oliveira et al. [111] have employed the following correlation suggested by Banerjee based on the large eddy model, to estimate the mass transfer coefficient in a continuous casting mold

$$k_m = 0.095u^*(Sc)^{-0.5}.(25) \quad (26)$$

where u^* is the friction velocity at the interface.

Xie and Oeters [124] followed a different approach to study a multi-reaction system. They applied the boundary layer theory and estimated the fluid's velocities using a relationship with the gas flow rate. The mass transfer coefficient for each one of the chemical species involved was defined by an equation of the form $k_i \propto Q^{0.168}$. Their model gave satisfactory agreement below the stirring energy for slag emulsification, the critical value was found in the order of 4 W/ton. This authors also discussed the effect of sulfur on the *mtc*. In one group of experiments sulphur increased the *mtc* but in another case its effect was null and they attributed this behavior to different concentrations of oxygen. The rate of desulphurization (DeS) is higher in low oxygen melts and this explains the two cases comparing Al and Si deoxidation. In Al-deoxidation melts the oxygen content is lower and gives higher rates of DeS. Jun et al. [125] and Ying [126] indicate that oxygen, which is a surfactant, retards the absorption of nitrogen because the surface velocity decreases due to the Marangoni effect. On the contrary, Mendes indicates that increasing the concentration of surfactants increase the rate of mass transfer due to an increase in interfacial convection [127]. This subject requires further investigation.

One of the limitations in developing mathematical models to define the *mtc* and its subsequent use to predict mass transfer rates, is the large computational time involved. Cao et al. [121] suggested to decouple the simultaneous computation of the *mtc* with a fluid flow model and the multi component reaction kinetics model in order to save time. Van Ende and Jung [94] opted for the use of a semiempirical relationship and even a number that just fits model predictions with experimental data [128].

In most of the previous work on mass transfer in metallurgical reactors it is assumed a homogeneous bath, but this is not entirely true, especially at the beginning of the process. The extent of homogenization depends on several factors such as the gas flow rate and injection layout. Mietz and Bruhl [129] studied the effect of the volume of dead zones on the mass transfer rates and found a large discrepancy comparing ideal mixing and real mixing conditions. Eventually, depending on the gas flow rate, the concentrations become similar when mixing is complete and the dead zones are decreased. However, since the time-scale for mixing time in water models or prototypes is in the order of seconds, varying from 10 to 180 s [130,131] and the time-scale for mass transfer is at least one order of magnitude higher, it is valid to assume an homogeneous concentration in mass transfer studies. In regard to the time-scale for mass transfer experiments in water models it is important to consider that the values reported are relative. We have carried out extensive work [132] that shows that the rate of mass transfer depends on many variables; gas flow rate, injection layout, physicochemical properties of phases involved, etc., therefore, the actual ratio between the two scales is variable.

It has been pointed out that the main purpose in defining the value of the *mtc's* is to use them in a kinetic model. It can be slag-metal refining, lime dissolution, formation mechanisms of non-metallic inclusions, etc. In the previous paragraphs some of the reports that have used mass transfer theories to compute the *mtc* have been mentioned. Table 4 summarizes how the *mtc* has been defined in different kinetic models.

Table 4. Methods employed to compute k in reported kinetic models.

Method	References
Correlation $k \propto \varepsilon^n$	Singh et al. [133], Zhang et al. [93], Van Ende and Jung [94]
Experimental work	Choi et al. [134], Harada et al. [135], Kang et al. [91], Roy et al. [136]
Correlations from D. Analysis	Wei et al. [137], Sulasalmi et al. [138], Huang et al. [139]
Boundary layer theory	Xie and Oeters [124], Chen et al. [140]
Higbie's penetration theory	Taniguchi et al. [119]
Large Eddy Model (LEM)	De Oliveira et al. [111], Deo and Grieveson [141],
Small Eddy Model (SEM)	Taniguchi et al. [119], Lou and Zhu [120], Cao et al. [121], Hoang et al. [122] and Karouni et al. [123]

It has also been mentioned before that the interfacial area is a variable difficult to measure. Without information of the real value, the volumetric mass transfer coefficient is reported instead. There are few reports about modeling the interfacial area during bottom gas injection. Cao et al. [121] reported a mathematical model that predicts the interfacial area. Their results indicate that the interfacial area is lower than the static area due to formation of the slag eye (s). Its value decreases as soon as the slag eye forms and tends to stabilize, showing a dynamic fluctuation depending on the formation slag droplets entrapped in liquid steel. This is true if there no slag emulsification included in the model. Sulasalmi et al. [138] reported a kinetic model incorporating the growth in interfacial area due to formation of slag droplets. Calculating the kinetics of emulsions requires the knowledge of the droplets residence time, its size distribution, and its generation rate. Unfortunately, very few investigations are currently available for kinetic models of slag–metal systems including the emulsification rate.

When the gas flow rate is increased there are two opposing effects, on one side, the slag droplets increase the interfacial area but also the area of the slag eye increases, decreasing the interfacial area. Zhang et al. [93] reported that bottom gas injection promotes the removal of non-metallic inclusions, however at a critical gas flow rate, due to the enlargement of the slag eye and the corresponding reoxidation, the amount of total oxygen increases, increasing again the amount of non-metallic inclusions. Lou and Zhu [120] also reported the existence of a maximum gas flow rate to reach the maximum rate of desulphurization, this value was reported to be 200 Nl/min in a ladle with 80 ton of liquid steel, equivalent to 7 Watt/ton. These results are extremely important because they clearly indicate the need to define limits to the maximum gas flow rate to reach the higher rate of mass transfer from impurities from liquid steel to the slag but taking also into consideration liquid steel reoxidation due to slag eye formation. Another solution is increasing from one to two porous plugs because in this way it is possible to increase the gas flow rate, increasing the interfacial area but also decreasing the slag-eye area [133].

5. Final Remarks

All the physical and mathematical modeling research involving liquid–liquid mass transfer due to bottom gas injection that has been described in this review has resulted in an extensive number of correlations that together with turbulence models and theories provide a solid understanding of the computation of the mass transfer coefficients, nevertheless, in spite of this progress no single equation includes all the variables that affect the rate of mass transfer and therefore they cannot provide a unified approach. Wilson and Macleod [142] presented a similar result in a review on gas–liquid mass transfer.

Based on this review it has been found that the following variables affect the mass transfer coefficient: (1) mass transfer is affected primarily by the gas flow rate, however, is not only the amount of stirring energy and flow velocities resulting from bottom gas injection that defines the value of the *mtc* but also; (2) how this gas is injected (number of nozzles, its radial position, type of nozzles and nozzle diameter), (3) the concentration of surfactants in the liquid phases, (4) slag emulsification (which

occurs above a critical gas flow rate) with its corresponding number of droplets, size and residence time, (5) interfacial area as a function of gas flow rate, (6) slag and steel physicochemical properties (diffusion coefficients, viscosity, relative densities, etc.), (7) bubble size and frequency, (8) reactor dimensions (diameter, height of the liquid, aspect ratio). From this list, gas flow rate and slag emulsification has been reported to have the largest influence. The author has argued that in the real steel/slag system slag emulsification in a ladle furnace can have a less significant role than is currently attributed because previous physical models have been developed using oils that do not represent the real slag phase. Slag emulsification in a ladle furnace is very important, however the upper limits of slag emulsification should be properly demonstrated by physical and mathematical modelling studies.

The correlations involving stirring energy and the *mtc* have been the most common but also the ones excluding most of the process variables affecting the rate of mass transfer. Dimensional analysis and mass transfer theories have included most of the relevant variables. Hirasawa et al. [59] reported the first attempt of a unified approach, however, their correlation does not include slag emulsification.

$$\frac{kd_c}{D} = C\left[\left(\frac{4Qd_c}{D\pi d_c^2}\right)\left(\frac{\rho g d_c^2}{\sigma}\right)\left(\frac{h}{d_c}\right)\right]^{\frac{1}{2}} \tag{27}$$

where C is a constant, h is the height of the liquid, σ is the interfacial tension.

In dimensionless form:

$$Sh = C'\left[(Pe)\left(\frac{\rho g d_c^2}{\sigma}\right)\left(\frac{d_B Re^{-n}}{d_c}\right)\right]^{\frac{1}{2}} \tag{28}$$

Reiter and Schwerdtfeger [143] also used dimensional analysis to describe mass transfer from bubbles in a thick upper phase, however this system is not representative of ladle furnace conditions.

Mathematical models involving CFD can estimate fluid flow patterns, with this information all the mass transfer theories can be applied to compute the *mtc*. It has been shown that in general all mass transfer theories can reproduce the experimental data, however, there is still some degree of empiricism with this approach. It is still necessary to adjust constants in those models.

Suggestions for future research: Future physical and mathematical modeling work to define the mass transfer coefficients in liquid–liquid mass transfer systems due to bottom gas injection should incorporate all the variables indicated previously, in particular those variables less studied; effect of nozzle radial position and separation angle, diameter and type of nozzles and the role of surfactants. In this effort dimensional analysis is most recommended. In physical modelling, proper similarity of slag emulsification with the real steel/slag system is needed in order to assess its real contribution to mass transfer. Mathematical modelling should incorporate a realistic approach as much as possible, which in addition to bubble size distribution should also evaluate the real contribution of slag emulsification and interfacial area under ladle furnace conditions. Once this work is completed, the final step will be to unify all experimental and numerical data.

The main purpose of bottom gas injection is to improve mixing phenomenon. The few experimental information available shows that a given injection layout can promote either mixing of liquid steel (by decreasing mixing time) or the rate of mass transfer (removal of impurities to the upper slag phase). One of the challenges ahead is to find conditions to improve both processes simultaneously.

Funding: This research received no external funding.

Acknowledgments: I want to acknowledge the support from the University of Science and Technology Beijing (USTB) to carry out this work during the pandemic of Coronavirus Covid-19.

Conflicts of Interest: The author declares no conflict of interest.

References

1. Mazumdar, D.; Guthrie, R.I.L. The Physical and Mathematical Modelling of Gas Stirred Ladle Systems. *ISIJ Int.* **1995**, *35*, 1–20. [CrossRef]
2. Mazumdar, D.; Evans, J.W. Macroscopic models for gas stirred ladles. *ISIJ Int.* **2004**, *44*, 447–461. [CrossRef]
3. Sichen, D. Modeling related to secondary steel making. *Steel Res. Int.* **2012**, *83*, 825–841. [CrossRef]
4. Liu, Y.; Ersson, M.; Liu, H.; Jönsson, P.G.; Gan, Y. A Review of Physical and Numerical Approaches for the Study of Gas Stirring in Ladle Metallurgy. *Metall. Mater. Trans. B Process Metall. Mater. Process. Sci.* **2019**, *50*, 555–577. [CrossRef]
5. Ghotli, R.A.; Abdul Aziz, A.R.; Ibrahim, S. Liquid-liquid mass transfer studies in various stirred vessel designs. *Rev. Chem. Eng.* **2015**, *31*, 329–343. [CrossRef]
6. Themelis, N.J. *Transport and Chemical Rate Phenomena*; Gordon and Breach: London, UK, 1995.
7. Veeraburus, M.; Philbrook, W.O. Observations on liquid-liquid mass transfer with bubble stirring. In *Physical Chemistry of Process Metallurgy*; Pierre, G.S., Ed.; Interscience: New York, NY, USA, 1959; p. 559.
8. Oeters, F.; Xie, H. Contribution to the theoretical description of metal-slag reaction kinetics. *Steel Res.* **1995**, *66*, 409–415. [CrossRef]
9. Gabe, D.R. The rotating cylinder electrode. *J. Appl. Electrochem.* **1974**, *4*, 91–108. [CrossRef]
10. Kosaka, M.; Minowa, S. Dissolution of Steel Cylinder into Liquid Fe-C Alloy. *Tetsu to Hagane* **1967**, *53*, 983–997. [CrossRef]
11. Kim, Y.U.; Pehlke, R.D. Mass Transfer During Dissolution of a Solid Into Liquid in the Iron-Carbon System. *Met. Trans* **1974**, *5*, 2527–2532. [CrossRef]
12. Shigeno, Y.; Tokuda, M.; Ohtani, M. The dissolution rate of graphite into Fe–C melt containing sulphur or phosphorus. *Trans. Japan. Inst. Met.* **1985**, *26*, 33–43. [CrossRef]
13. Szekely, J.; Lehner, T.; Chang, C.W. Flow Phenomena Mixing and Mass Transfer in Argon-Stirred Ladles. *Ironmak. Steelmak.* **1979**, *7*, 285–293.
14. Mazumdar, D.; Kajani, S.K.; Ghosh, A. Mass transfer between solid and liquid in vessels agitated by bubble plume. *Steel Res.* **1990**, *61*, 339–346. [CrossRef]
15. Mazumdar, D.; Narayan, T.; Bansal, P. Mathematical modelling of mass transfer rates between solid and liquid in high-temperature gas-stirred melts. *Appl. Math. Model.* **1992**, *16*, 255–262. [CrossRef]
16. Szekely, J.; Grevet, H.H.; El-Kaddah, N. Melting rates in turbulent recirculating flow systems. *Int. J. Heat Mass Transf.* **1984**, *27*, 1116–1121. [CrossRef]
17. Singh, A.K.; Mazumdar, D. Mass transfer between solid and liquid in a gas-stirred vessel. *Metall. Mater. Trans. B Process Metall. Mater. Process. Sci.* **1997**, *28*, 95–102. [CrossRef]
18. Taniguchi, S.; Ohmi, M.; Ishiura, S.; Yamauchi, S. Cold model study on the effect of gas injection upon the melting rate of a solid sphere in a liquid bath. *Trans. Iron Steel Inst. Japan* **1983**, *23*, 565–570. [CrossRef]
19. Koria, S.C. Model investigations on liquid velocity induced by submerged gas injection in steel bath. *Steel Res.* **1988**, *59*, 484–491. [CrossRef]
20. Matsushima, M.; Yadoomaru, S.; Mori, K.; Kawai, Y. A Fundamental Study on the Dissolution Rate of Solid Lime into Liquid Slag. *Trans. Iron Steel Inst. Japan* **1977**, *17*, 442–449. [CrossRef]
21. Taira, S.; Nakashima, K.; Mori, K. Kinetic Behavior of Dissolution of Sintered Alumina Into Cao-Si02&Al203 Slags. *ISIJ Int.* **1993**, *33*, 116–123.
22. Kitamura, S.; Shibata, H.; Maruoka, N. Kinetic Model of Hot Metal Dephosphorization by Liquid and Solid Coexisting Slags. *Steel Res. Int.* **2008**, *79*, 586–590. [CrossRef]
23. Wright, J.K. Steel dissolution in quiescent and gas stirred Fe/C melts. *Metall. Trans. B* **1989**, *20*, 363–374. [CrossRef]
24. Maruoka, N.; Lazuardi, F.; Maeyama, T.; Kim, S.-J.; Conejo, A.N.; Shibata, H.; Kitamura, S.-Y. Evaluation of bubble eye area to improve gas/liquid reaction rates at bath surfaces. *ISIJ Int.* **2011**, *51*, 236–241. [CrossRef]
25. Kato, Y.; Fujii, T.S.; Habu, Y. Gas-liquid mass transfer of bottom and top blowing in comverters by water modeling. *Testu to Hagane* **1983**, *69*, S1011.
26. Inada, S.; Watanabe, T. The Model Experiment on the Reaction between the Liquid and the Swarms of Gas Bubbles by NaOH-CO2 System. *Tetsu to Hagane* **1977**, *63*, 37–44. [CrossRef]
27. Sakaguchi, K.; Ito, K. Measurement of the Volumetric Mass Transfer Coefficient of Gas-stirred Vessel under Reduced Pressure. *ISIJ Int.* **1995**, *35*, 1348–1353. [CrossRef]

28. Rui, Q.; Jiang, F.; Ma, Z.; You, Z.; Cheng, G.; Zhang, J. Effect of elliptical snorkel on the decarburization rate in single snorkel refining furnace. *Steel Res. Int.* **2013**, *84*, 192–197. [CrossRef]
29. Subramanian, N.; Richardson, F.D. Mass transfer across interfaces agitated by large bubbles. *JISI* **1968**, *June*, 576–583.
30. Richardson, F.D.; Robertson, D.G.C.; Staples, B.B. Mass Transfer Across Metal/Slag Interfaces Stirred by Bubbles. In Proceedings of the The Darken Conference on Physical Chemistry in Metallurgy, Pittsburgh, PA, USA, 23–25 August 1976; pp. 25–48.
31. Li, X.; Yin, Z. Mass transfer to liquid-liquid interface. *Acta Metall. Sin.* **1996**, *9*, 151–156.
32. Fruehan, R.J.; Martonik, L.K. Physical Behavior and Liquid-Phase Mass Transfer of Submerged Gas Jets in Liquids. In Proceedings of the 3rd International Iron and Steel Congres, Chicago, IL, USA, 16–20 April 1978; pp. 229–238.
33. Riboud, O.V.; Olette, M. Mechanisms of some of the reactions involved in secondary refining. In Proceedings of the 7th International Conference on Vacuum Metallurgy (ICVM), Tokyo, Japan, 26–30 November 1982; pp. 879–889.
34. Gaye, H.; Gatellier, C.; Riboud, P.V. Physico-Chemical Aspects of the Ladle Desulphurization of Iron and Steel. *Foundry Process.* **1988**, 333–356.
35. Nakanishi, K.; Fujii, T.; Szekely, J. Possible relationship between energy dissipation and agitation in steel-processing operations. *Ironmak. Steelmak.* **1975**, *2*, 193–197.
36. Ilegbusi, O.J. Role of gas plumes in agitation and mass transfer in metallurgical systems. *Steel Res.* **1994**, *65*, 534–540. [CrossRef]
37. Asai, S.; Kawachi, M.; Muchi, I. Mass transfer rate in ladle refining processes. In *SCANINJECT III: Proceedings of the Refining of Iron and Steel by Powder Injection, Lulea Sweden, 15–17 June 1983*; MEFOS: Lulea, Sweden, 1983; pp. 12:1–12:29.
38. Lehner, T.; Carlsson, G.; Hsiao, T.C. On Fluid Flow and Metallurgical Reaction in Gas Stirred Melts. In *SCANINJECT II: Proceedings of the 2nd International Conference on Injection Metallurgy, Lulea, Sweden, 12–13 June 1980*; MEFOS: Lulea, Sweden, 1980; Article 22.
39. Engh, T.A. *Principles of Metal Refining*; Oxford University Press: Oxford, UK, 1992.
40. Oeters, F. *Metallurgy of Steelmaking*; Verlag Stahleisen mbH: Dusseldorf, Germany, 1994.
41. Conejo, A.N.; Lara, F.R.; Macias-Hernández, M.; Morales, R.D. Kinetic model of steel refining in a ladle furnace. *Steel Res. Int.* **2007**, *78*, 141–150. [CrossRef]
42. Mazumdar, D.; Guthrie, R.I.L. Mixing models for gas stirred metallurgical reactors. *Metall. Trans. B* **1986**, *17*, 725–733. [CrossRef]
43. Nakanishi, K.; Kato, Y.; Nozaki, T.; Emi, T. Cold Model Study on the Mixing Rates of Slag and Metal Bath in Q-Bop. *Tetsu-To-Hagane* **1980**, *66*, 1307–1316. [CrossRef]
44. Ishida, J.; Yamaguchi, K.; Sugiura, S.; Yamano, K.; Hayakawa, S.; Demukai, N. Effects of Stirring by Argon Gas Injection on Metallurgical Reactions in Secondary Steelmaking. *Denki-Seiko (Electric Furn. Steel)* **1981**, *52*, 2–8.
45. Berg, B.; Carlsson, G.; Bramming, M. Ladle Metallurgy-Influence of Different Stirring Methods. *Scand. J. Met.* **1985**, *14*, 299–305.
46. Umezawa, K.; Nishugi, S.; Arima, R.; Matsunaga, H. Development of De-P and De-S treatment methods for powder injection with CaO flux. *Testu to Hagane* **1981**, *67*, S182.
47. Umezawa, K.; Matsunaga, H.; Arima, R.; Tonomura, S.; Furugaki, I. The Influence of Operating Condition on Dephosphorization and Desulphurization Reactions of Hot Metal with Lime-based Flux. *Tetsu to Hagane* **1983**, *69*, 1810–1817. [CrossRef]
48. Clinton, S.D.; Perona, J.J. Mass Transfer in a Bubble-Agitated Liquid-Liquid System. *Ind. Eng. Chem. Fundamen.* **1982**, 269–271. [CrossRef]
49. Minda, A.Y.S.; Asaho, R.; Komamura, K.; Kato, Y. Study of stainless steel smelting by top blowing. *Testu to Hagane* **1983**, *69*, S1007.
50. Asai, S.; Muchi, I.; Kawachi, M. Fluid Flow and Mass Transfer in Gas Stirred Ladles. *Foundry Process.* **1988**, 261–292.
51. Patel, P.; Frohberg, M.G.; Papamantellos, D. Experimental studies of mass transfer between two immiscible liquids. *Trans. AIME* **1969**, *245*, 855–859.
52. Sawada, I.; Ohashi, T.; Kajioka, H. Mass transfer rate between slag and metal in a ladle due to bottom gas injection. *Tetsu to Hagane* **1984**, *70*, S161.

53. Ooga, Y.; Taniguchi, S.; Kikuchi, J. Fundamental research on the behavior of liquid-liquid substances under gas stirring. *Tetsu to Hagane* **1985**, *71*, S897.
54. Endo, S.; Hasegawa, M. Cold model study on effect of stirring on slag metal reaction. *Tetsu to Hagane* **1985**, *71*, S899.
55. Hirasawa, M.; Mori, K.; Sano, M.; Shimatani, Y.; Okazaki, Y. Effect of gas flow rate on slag/metal mass transfer. *Tetsu to Hagane* **1985**, *71*, S898.
56. Hirasawa, M.; Mori, K.; Sano, M.; Hatanaka, A.; Shimatani, Y.; Okazaki, Y. Kinetic Studies on the Rate of Reaction Between Molten Slag and Metal With Gas-Injection Stirring. *Tetsu to Hagane* **1987**, *73*, 1343–1349. [CrossRef]
57. Hirasawa, M.; Mori, K.; Sano, M.; Hatanaka, A.; Shimatani, Y.; Okazaki, Y. The Analysis System of Metal-side Stirring in a Slag-Metal Reaction with Gas-injection. *Testu to Hagane* **1987**, *73*, 1350–1357. [CrossRef]
58. Hirasawa, M.; Mori, K.; Sano, M.; Hatanaka, A.; Shimatani, Y.; Okazaki, Y. Rate of Mass Transfer Between Molten Slag and Metal Under Gas Injection Stirring. *Trans. ISIJ* **1987**, *27*, 277–282. [CrossRef]
59. Hirasawa, M.; Mori, K.; Sano, M.; Shimatani, Y.; Okazaki, Y. Correlation Equations for Metal-Side Mass Transfer in a Slag-Metal Reaction System With Gas Injection Stirring. *Trans. ISIJ* **1987**, *27*, 283–290. [CrossRef]
60. Mukawa, S.; Mizukami, Y. Effect of Stirring Energy and Rate of Oxygen Supply on the Rate of Hot Metal Dephosphorization. *ISIJ Int.* **1995**, *35*, 1374–1380. [CrossRef]
61. Kim, S.H.; Fruehan, R.J. Physical modeling of gas/liquid mass transfer in a gas stirred ladle. *Metall. Trans. B* **1987**, *18*, 673–680. [CrossRef]
62. Matway, R.J.; Fruehan, R.J.; Henein, H. Physical Modeling of Gas Injection in a Steelmaking Vessel-Mixing Times and Liquid/Liquid Mass Transfer Rates. *Iron Steelmak.* **1989**, *16*, 51–58.
63. Matway, R.J.; Fruehan, R.J.; Henein, H. Physical Modeling of Slag/Metal Reactions in Combined Blowing-Effect of Tuyere Location, Tuyere Size, and Gas Flowrate. *Iron Steelmak.* **1991**, *18*, 43–50.
64. Singh, V.; Lenka, S.N.; Ajmani, S.K.; Bhanu, C.; Pathak, S. A novel bottom stirring scheme to improve BOF performance through mixing and mass transfer modelling. *ISIJ Int.* **2009**, *49*, 1889–1894. [CrossRef]
65. Mietz, J.; Schneider, S.; Oeters, F. Model experiments on mass transfer in ladle metallurgy. *Steel Res.* **1991**, *62*, 1–9. [CrossRef]
66. Mietz, J.; Schneider, S.; Oeters, F. Emulsification and mass transfer in ladle metallurgy. *Steel Res.* **1991**, *62*, 10–15. [CrossRef]
67. Lou, W.; Zhu, M. Numerical simulation of slag-metal reactions and desulfurization efficiency in gas-stirred ladles with different thermodynamics and kinetics. *ISIJ Int.* **2015**, *55*, 961–969. [CrossRef]
68. Koria, S.C.; George, A. Selection of bottom injection parameters in combined blown steelmaking. *Ironmak. Steelmak.* **1988**, *15*, 127–133.
69. Koria, S.C.; Pal, S. Model study on mixing condition in combined blown steelmaking bath. *Ironmak. Steelmak.* **1990**, *17*, 325–332.
70. Koria, S.C.; Shamsi, M. Simulation of mass transfer from metal to slag in gas stirred ladles. *Ironmak. Steelmak.* **1990**, *17*, 401–409.
71. Deng, J.; Oeters, F. Mass transfer of sulfur from liquid iron into lime-saturated CaO-Al2O3-MgO-SiO2 slags. *Steel Res.* **1990**, *61*, 438–448. [CrossRef]
72. Kitamura, S.Y.; Kitamura, T.; Shibata, K.; Mizukami, Y.; Mukawa, S.; Nakagawa, J. Effect of Stirring Energy, Temperature and Flux Composition on Hot Metal Dephosphorization Kinetics. *ISIJ Int.* **1991**, *31*, 1322–1328. [CrossRef]
73. Koria, S.C. Studies of the bath mixing intensity in converter steelmaking processes. *Can. Metall. Q.* **1992**, *31*, 105–112. [CrossRef]
74. Lachmund, H.; Xie, Y.; Harste, K. Thermodynamic and kinetic aspects of the desulphurisation reaction in secondary metallurgy. *Steel Res.* **2001**, *72*, 452–459. [CrossRef]
75. Lachmund, H.; Xie, Y.; Buhles, T.; Pluschkell, W. Slag emulsification during liquid steel desulphurisation by gas injection into the ladle. *Steel Res.* **2003**, *74*, 77–85. [CrossRef]
76. Sulasalmi, P.; Visuri, V.V.; Kärnä, A.; Fabritius, T. Simulation of the effect of steel flow velocity on slag droplet distribution and interfacial area between steel and slag. *Steel Res. Int.* **2015**, *86*, 212–222. [CrossRef]
77. Senguttuvan, A.; Irons, G.A. Modeling of slag entrainment and interfacial mass transfer in gas stirred ladles. *ISIJ Int.* **2017**, *57*, 1962–1970. [CrossRef]

78. Stapurewicz, T.; Themelis, N.J. Mixing and mass transfer phenomena in bottom-injected gas-liquid reactors. *Can. Metall. Q.* **1987**, *26*, 123–128. [CrossRef]
79. Terrazas, M.S.C.; Conejo, A.N. Effect of nozzle diameter, nozzle radial position and a top slag layer on mixing time during bottom gas injection in metallurgical ladles. In Proceedings of the 6th International Congress on the Science and Technology of Steelmaking (ICS 2015), Beijing, China, 12–14 May 2015.
80. Mori, K. Kinetics of Fundamental Reactions Pertinent To Steelmaking Process. *Trans. Iron Steel Inst. Japan* **1988**, *28*, 246–261. [CrossRef]
81. Joo, S.; Guthrie, R.I.L. Modeling flows and mixing in steelmaking ladles designed for single- and dual-plug bubbling operations. *Metall. Trans. B* **1992**, *23*, 765–778. [CrossRef]
82. Wei, T.; Oeters, F. Model test for emulsion in gas-stirred ladles. *Steel Res.* **1992**, *63*, 60–68. [CrossRef]
83. Savolainen, J.; Fabritius, T.; Mattila, O. Effect of fluid physical properties on the emulsification. *ISIJ Int.* **2009**, *49*, 29–36. [CrossRef]
84. Hatch, G.G.; Chipman, J. Sulphur Equilibria between Iron Blast Furnace Slags and Metal. *JOM* **1949**, *1*, 274–284. [CrossRef]
85. Simeonov, S.; Ivanchev, I.; Hainadjiev, A. Sulphur equilibrium distribution between CaO-CaF2-Si02-Al203 slags and carbon-saturated iron. *ISIJ Int.* **1991**, *31*, 1396–1399. [CrossRef]
86. Andersson, M.; Hallberg, M.; Jonsson, L.; Jönsson, P. Slag-metal reactions during ladle treatment with focus on desulphurisation. *Ironmak. Steelmak.* **2002**, *29*, 224–232. [CrossRef]
87. Sardar, M.K.; Mukhopadhyay, S.; Majumder, S.; Mallick, S.; Singh, R.K. Effect of plug location on desulfurization characteristics of slag during ladle furnace operation. *Can. Metall. Q.* **2006**, *45*, 175–180. [CrossRef]
88. Lehrer, L.H. Gas agitation of liquids. *Ind. Eng. Chem. Process Des. Dev.* **1968**, *7*, 226–239. [CrossRef]
89. Jiang, F.; Song, Y.X.; Cheng, G.G. Effect of orifice configuration on the volumetric mass transfer coefficient during ladle purging. *Rev. Metall.* **2011**, *108*, 465–472. [CrossRef]
90. Robison, J.W.; Pehlke, R.D. Kinetics of Chromium Oxide Reduction From a Basic Steelmaking Slag By Silicon Dissolved in Liquid Iron. *Met. Trans* **1974**, *5*, 1041–1051. [CrossRef]
91. Kang, Y.B.; Kim, M.S.; Lee, S.W.; Cho, J.W.; Park, M.S.; Lee, H.G. A reaction between high Mn-High Al Steel and CaO-SiO2-Type molten mold flux: Part II. reaction mechanism, interface morphology, and Al 2O3 accumulation in molten mold flux. *Metall. Mater. Trans. B Process Metall. Mater. Process. Sci.* **2013**, *44*, 309–316. [CrossRef]
92. Conejo, A.N.; Kitamura, S.; Maruoka, N.; Kim, S.-J. Effects of top layer, nozzle arrangement, and gas flow rate on mixing time in agitated ladles by bottom gas injection. *Metall. Mater. Trans. B Process Metall. Mater. Process. Sci.* **2013**, *44*, 914–923. [CrossRef]
93. Zhang, Y.; Ren, Y.; Zhang, L. Kinetic study on compositional variations of inclusions, steel and slag during refining process. *Metall. Res. Technol.* **2018**, *115*, 415. [CrossRef]
94. Van Ende, M.A.; Jung, I.H. A Kinetic Ladle Furnace Process Simulation Model: Effective Equilibrium Reaction Zone Model Using FactSage Macro Processing. *Metall. Mater. Trans. B Process Metall. Mater. Process. Sci.* **2017**, *48*, 28–36. [CrossRef]
95. Lewis, W.K.; Whitman, W.G. Principles of Gas Absorption. *Ind. Eng. Chem.* **1924**, *16*, 1215–1220. [CrossRef]
96. Kang, J.G.; Shin, J.H.; Chung, Y.; Park, J.H. Effect of Slag Chemistry on the Desulfurization Kinetics in Secondary Refining Processes. *Metall. Mater. Trans. B Process Metall. Mater. Process. Sci.* **2017**, *48*, 2123–2135. [CrossRef]
97. Deo, B.; Boom, R. *Fundamentals of Steelmaking Metallurgy*, 1st ed.; Prentice-Hall: New York, NY, USA, 1993.
98. Higbie, R. The rate of absorption of a pure gas into a still liquid. *Trans. Am. Inst. Chem. Eng.* **1935**, *35*, 36–60.
99. Szekely, J. Mathematical model for heat or mass transfer at the bubble-stirred interface of two immiscible liquids. *Int. J. Heat Mass Transf.* **1963**, *6*, 417–422. [CrossRef]
100. Bafghi, M.S.; Kurimoto, H.; Sano, M. Effect of Slag Foaming on the Reduction of Iron Oxide in Molten Slag by Graphite. *ISIJ Int.* **1992**, *32*, 1084–1090. [CrossRef]
101. Danckwerts, P.V. Significance of liquid-film coefficients in gas absorption. *Eng. Process Dev.* **1951**, *43*, 1460–1467. [CrossRef]
102. Dong, L.; Johansen, S.T.; Engh, T.A. Mass transfer at gas-liquid interfaces in stirred vessels. *Can. Metall. Q.* **1992**, *31*, 299–307. [CrossRef]

103. Fortescue, G.E.; Pearson, J.R.A. Gas absorption into a turbulent liquid. *Chem. Eng. Sci.* **1967**, *22*, 1163–1176. [CrossRef]
104. Kolmogorov, A.N. The local structure of turbulence in incompressible viscous fluid for very large Reynolds number. *Dokl. Akad. Nauk SSSR* **1941**, *30*, 538–540.
105. Banerjee, S.; Rhodes, E.; Scott, D.S. Mass transfer to falling wavy liquid films in turbulent flow. *Eng. Chem. Fundam.* **1968**, *7*, 22–27. [CrossRef]
106. Lamont, J.C.; Scott, D.S. An eddy cell model of mass transfer into the surface of a turbulent liquid. *AIChE J.* **1970**, *16*, 513–519. [CrossRef]
107. Miyauchi, T.; Kataoka, H. Liquid film coefficient of mass transfer on free liquid surface. *J. Chem. Eng. Japan* **1970**, *3*, 257–258. [CrossRef]
108. Ruckenstein, E. Physical Models for Mass or Heat Transfer Processes. *Int Chem. Eng.* **1967**, *7*, 490.
109. Banerjee, S.; Lakehal, D.; Fulgosi, M. Surface divergence models for scalar exchange between turbulent streams. *Int. J. Multiph. Flow* **2004**, *30*, 963–977. [CrossRef]
110. Theofanous, T.G.; Houze, R.N.; Brumfield, L.K. Turbulent mass transfer at free, gas-liquid interfaces, with applications to open-channel, bubble and jet flows. *Int. J. Heat Mass Transf.* **1976**, *19*, 613–624. [CrossRef]
111. De Oliveira Campos, L.D. *Mass Transfer Coefficients across Dynamic Liquid Steel/Slag Interface*; L'Université de Bordeaux: Bordeaux, France, 2017.
112. Duan, H.; Zhang, L.; Thomas, B.G.; Conejo, A.N. Fluid Flow, Dissolution, and Mixing Phenomena in Argon-Stirred Steel Ladles. *Metall. Mater. Trans. B Process Metall. Mater. Process. Sci.* **2018**, *49*, 2722–2743. [CrossRef]
113. Cloete, S.W.P.; Eksteen, J.J.; Bradshaw, S.M. A mathematical modelling study of fluid flow and mixing in full-scale gas-stirred ladles. *Prog. Comput. Fluid Dyna mics* **2009**, *9*, 345–356. [CrossRef]
114. Costa, L.T.; Tavares, R.P. Multiphase Mass Mass Transfer in Iron and Steel Refining Processes. In *Mass Transfer—Advancement in Process Modelling*; Solecki, M., Ed.; InTech Open: London, UK, 2015; pp. 149–187. ISBN 9789535121923.
115. Seyed Ahmadi, M.; Argyropoulos, S.A.; Bussmann, M.; Doutre, D. Comparative Studies of Silicon Dissolution in Molten Aluminum Under Different Flow Conditions, Part I: Single-Phase Flow. *Metall. Mater. Trans. B Process Metall. Mater. Process. Sci.* **2015**, *46*, 1275–1289. [CrossRef]
116. Seyed Ahmadi, M.; Argyropoulos, S.A.; Bussmann, M.; Doutre, D. Comparative Studies of Silicon Dissolution in Molten Aluminum Under Different Flow Conditions Part II: Two-Phase Flow. *Metall. Mater. Trans. B* **2015**, *46*, 1290–1301. [CrossRef]
117. Seyed Ahmadi, M.; Bussmann, M.; Argyropoulos, S.A. Mass transfer correlations for dissolution of cylindrical additions in liquid metals with gas agitation. *Int. J. Heat Mass Transf.* **2016**, *97*, 767–778. [CrossRef]
118. Churchill, S.W.; Bernstein, M. A correlating equation for forced convection from gases and liquids to a circular cylinder in crossflow. *J. Heat Transfer* **1977**, *99*, 300–306. [CrossRef]
119. Taniguchi, S.; Kawaguchi, S.; Kikuchi, A. Fluid flow and gas-liquid mass transfer in gas-injected vessels. *Appl. Math. Model.* **2002**, *26*, 249–262. [CrossRef]
120. Lou, W.; Zhu, M. Numerical Simulation of Desulfurization Behavior in Gas-Stirred Systems Based on Computation Fluid Dynamics–Simultaneous Reaction Model (CFD–SRM) Coupled Model. *Metall. Mater. Trans. B Process Metall. Mater. Process. Sci.* **2014**, *45*, 1706–1722. [CrossRef]
121. Cao, Q.; Nastac, L.; Pitts-Baggett, A.; Yu, Q. Numerical Investigation of Desulfurization Kinetics in Gas-Stirred Ladles by a Quick Modeling Analysis Approach. *Metall. Mater. Trans. B Process Metall. Mater. Process. Sci.* **2018**, *49*, 988–1002. [CrossRef]
122. Hoang, Q.N.; Ramírez-Argáez, M.A.; Conejo, A.N.; Blanpain, B.; Dutta, A. Numerical Modeling of Liquid–Liquid Mass Transfer and the Influence of Mixing in Gas-Stirred Ladles. *JOM* **2018**, *70*, 2109–2118. [CrossRef]
123. Karouni, F.; Wynne, B.P.; Talamantes-Silva, J.; Phillips, S. Hydrogen Degassing in a Vacuum Arc Degasser Using a Three-Phase Eulerian Method and Discrete Population Balance Model. *Steel Res. Int.* **2018**, *89*, 1–11. [CrossRef]
124. Xie, H.; Oeters, F. Kinetics of mass transfer of manganese and silicon between liquid iron and slags. *Steel Res.* **1995**, *66*, 501–508. [CrossRef]

125. Jun, Z.; Shi, F.; Mukai, K.; Tsukamoto, H. Numerical analysis of nitrogen absorption rate accompanied with Marangoni convection in the molten iron under non-inductive stirring condition. *ISIJ Int.* **1999**, *39*, 409–418. [CrossRef]
126. Ying, Q. Mass Transfer Coefficients in Metallurgical Reactors. *J. Univ. Sci. Technol. 10* **2010**, *2*, 1–9.
127. Mendes, M.A. Surfactant Effects on Mass Transfer in Liquid-Liquid Systems. *Fluid Mech. Surfactant Polym. Solut.* **2004**, 39–56.
128. Pirker, S.; Gittler, P.; Pirker, H.; Lehner, J. CFD, a design tool for a new hot metal desulfurization technology. *Appl. Math. Model.* **2002**, *26*, 337–350. [CrossRef]
129. Mietz, J.; Bruhl, M. Model calculations for mass transfer with mixing in ladle metallurgy. *Steel Res.* **1990**, *61*, 105–112. [CrossRef]
130. Terrazas, M.S.C.; Conejo, A.N. Effect of Nozzle Diameter on Mixing Time During Bottom-Gas Injection in Metallurgical Ladles. *Metall. Mater. Trans. B Process Metall. Mater. Process. Sci.* **2015**, *46*, 711–718. [CrossRef]
131. Nuñez, D.A.; Ramirez-Argaez, M.A.; Conejo, A.N. Mathematical modeling of bottom gas injection in industrial metallurgical ladles in the presence of a top layer of slag. In Proceedings of the 8th Pacific Rim International Congress on Advanced Materials and Processing 2013 (PRICM 8), Waikoloa, HI, USA, 4–9 August 2013; Volume 4.
132. Likhachou, P.; Conejo, A. *Mass Transfer in Ladles Due to Bottom Gas Injection. Research in progress*, Beijing, China. 2020.
133. Singh, U.; Anapagaddi, R.; Mangal, S.; Padmanabhan, K.A.; Singh, A.K. Multiphase Modeling of Bottom-Stirred Ladle for Prediction of Slag–Steel Interface and Estimation of Desulfurization Behavior. *Metall. Mater. Trans. B Process Metall. Mater. Process. Sci.* **2016**, *47*, 1804–1816. [CrossRef]
134. Choi, J.Y.; Kim, D.J.; Lee, H.G. Reaction kinetics of desulfurization of molten pig iron using CaO-SiO2-Al2O3-Na2O slag systems. *ISIJ Int.* **2001**, *41*, 216–224. [CrossRef]
135. Harada, A.; Maruoka, N.; Shibata, H.; Kitamura, S.Y. A kinetic model to predict the compositions of metal, slag and inclusions during ladle refining: Part1. Basic Concept and Application. *ISIJ Int.* **2013**, *53*, 2110–2117. [CrossRef]
136. Roy, D.; Pistorius, P.C.; Fruehan, R.J. Effect of silicon on the desulfurization of Al-killed steels: Part II. Experimental results and plant trials. *Metall. Mater. Trans. B Process Metall. Mater. Process. Sci.* **2013**, *44*, 1095–1104. [CrossRef]
137. Wei, J.H.; Zhu, S.J.; Yu, N.W. Kinetic model of desulphurization by powder injection and blowing in RH refining of molten steel. *Ironmak. Steelmak.* **2000**, *27*, 129–137. [CrossRef]
138. Sulasalmi, P.; Visuri, V.V.; Kärnä, A.; Järvinen, M.; Ollila, S.; Fabritius, T. A Mathematical Model for the Reduction Stage of the CAS-OB Process. *Metall. Mater. Trans. B Process Metall. Mater. Process. Sci.* **2016**, *47*, 3544–3556. [CrossRef]
139. Huang, F.; Zhang, L.; Zhang, Y.; Ren, Y. Kinetic Modeling for the Dissolution of MgO Lining Refractory in Al-Killed Steels. *Metall. Mater. Trans. B Process Metall. Mater. Process. Sci.* **2017**, *48*, 2195–2206. [CrossRef]
140. Chen, Y.N.C.; Bao, Y.P.; Wang, M.; Zhao, L.H.; Peng, Z. A mathematical model for the dynamic desulfurization process of ultra-low-sulfur steel in the LF refining process. *Metall. Res. Technol.* **2014**, *111*, 37–43. [CrossRef]
141. Deo, B.; Grieveson, P. Kinetics of desulphurisation of molten pig iron. *Steel Res.* **1986**, *57*, 514–519. [CrossRef]
142. Wilson, G.T.; MacLeod, N. A critical appraisal of empirical equations and models for the prediction of the coefficient of reaeration of deoxygenated water. *Water Res.* **1974**, *8*, 341–366. [CrossRef]
143. Reiter, G.; Schwerdtfeger, K. Characteristics of Entrainment at Liquid/Liquid Interfaces due to Rising Bubbles. *ISIJ Int.* **1992**, *32*, 57–65. [CrossRef]